Díaz-Rey, MDR.; Paris-Carrizo, CG.; Martinez Franco, R.; Moliner Marin, M.; Martínez, C.; Corma Canós, A. (2017). Efficient Oligomerization of Pentene into Liquid Fuels on Nanocrystalline Beta Zeolites. ACS Catalysis. 7(9):6170-6178. doi:10.1021/acscatal.7b00817

Efficient Oligomerization of Pentene into Liquid Fuels on Nanocrystalline Beta Zeolites

M. Rocío Díaz-Rey, Cecilia Paris, Raquel Martínez-Franco, Manuel Moliner, Cristina Martínez, Avelino Corma**

Instituto de Tecnología Química, Universitat Politècnica de València-Consejo Superior de Investigaciones Científicas, Avenida de los Naranjos s/n, 46022 València, Spain.

Corresponding Authors:

*E-mail: acorma@itq.upv.es; cmsanche@itq.upv.es.

ABSTRACT

Light alkenes oligomerization, performed in the presence of heterogeneous acid catalysts, is an interesting alternative for the production of clean liquid fuels. The process, when catalyzed by zeolites, is flexible and can be directed to the formation of oligomers in the gasoline, jet fuel or diesel range by adjusting the reaction conditions and the zeolite's structure. Herein we show how reducing the crystal size of large pore Beta zeolites down to 10-15 nm and controlling the number and strength distribution of their Brønsted acid sites leads to highly active and stable catalysts, selective to true oligomers within the naphtha and, especially, the diesel range. The shorter diffusion path lengths in the smaller crystallites and the reduced Brønsted acid site density of the two nanosized beta zeolites (10-15 nm) synthesized with Si/Al=15 lead to 1-pentene conversion above 80% during the six hours time on stream (TOS) at a space time (W/F) of 2.8 $g \cdot h \cdot mol^{-1}$. This value is

higher than the olefin conversion obtained for a commercial nanobeta (30 nm) at a threefold space time of 9.1 $g \cdot h \cdot mol^{-1}$.

KEYWORDS: Nano-zeolite, beta [BEA], dicationic OSDA, olefin oligomerization, catalyst deactivation.

INTRODUCTION

Oligomerization of light olefins is a well-known, efficient technology for producing environmentally friendly synthetic fuels, such as gasoline, jet fuel and diesel, free of sulfur and aromatics[1-3]. This process is even more attractive when the light olefins, which could range between the C_3 and C_6 fractions, belong to orphan or low value refinery streams, such as naphthas produced by catalytic cracking (FCC)[4] or Fischer-Tropsch tail gas, especially the one derived from low temperature facilities, more diluted and often not processed for olefin recovery[5]. Light olefins produced from biorenewable sources[6] or present in natural gas obtained by fracking are also potential feedstocks to be upgraded in this way[7].

Along the last decade there has been increasing interest in converting light naphtha streams, too high in Reid vapor pressure to be blend directly into the gasoline pool in significant amounts, to heavier products. In particular, oligomerization of the Light Cracked Naphtha (LCN) stream produced in the FCC unit, rich in C_5 and C_6 alkenes, is an interesting alternative to other refinery strategies such as alkylation or cracking[8].

Oligomerization of alkenes can be catalyzed by Brønsted acid sites, and different solid acids have been described for this purpose. Phosphoric acid supported on silica (also known as solid phosphoric acid -SPA-) was the first industrial oligomerization catalyst,

developed by UOP in 1935[9]. However, this phosphoric-based catalyst presents different drawbacks, such as its limited tolerance to feed hydration level, its relatively short catalyst lifetime and the environmental and corrosion problems associated with the use of the inorganic acid[10-12]. In addition, the high branching degree of the products makes this process not suitable for the production of diesel and limits it to gasoline fractions[13]. Thus, the design of alternative, more efficient heterogeneous oligomerization catalysts has received a significant attention for years[14-18]. In the 1980s, Mobil researchers developed a heterogeneous catalyst based on a ZSM-5 zeolite, which allowed producing oligomers within the gasoline or the diesel fraction, just by adjusting the operation conditions of their MOGD process[19]. The medium pores of the MFI structure, with pore openings of ~5.5 Å, restricted the branching degree of the products by shape-selectivity favoring the formation of methyl-branched oligomers[20]. This discovery paved the way for numerous studies on the effect of the zeolite pore structure for the light olefins oligomerization reaction[2, 16-18, 21-23]. The large versatility in the synthesis of zeolites, which can be prepared with different pore structure and size or with flexible chemical composition and acidic properties, among others, can lead to zeolite based catalysts with maximum selectivity towards the desired products, or improved catalyst lifetime by optimization of their physico-chemical properties.[21, 24-25]

In general, it has been observed that medium pore zeolites produce more linear hydrocarbons with less branched alkyl groups than large pore zeolites, making them, therefore, especially adequate for the production of high quality diesel fractions[14-19, 26]. In addition, these medium pore zeolites largely preclude the formation of heavier oligomers and aromatic products, which would lead to relative fast catalyst deactivation by coke deposition, and present, therefore, longer catalyst life[11-12]. Taking this into account, and considering that the present market trends, especially in Europe, demand more diesel than

gasoline, one of the most active research tasks in the olefin oligomerization field has been focused on the study and optimization of the properties of medium-pore zeolites, and in particular ZSM-5[16, 22-23, 26]. Zeolites with one-dimensional pore structures, such as TON or MTW have been reported to enhance the linearity of the oligomers, and therefore the quality of the resulting diesel fraction, even more[8, 27-30], but diffusion limitations strongly reduce the catalytic efficiency, especially for C_5-C_6 olefins, unless diffusion paths are reduced, for instance, by means of post-synthesis mesoporosity generation[27]. On the other hand, large pore 3D zeolites tend to favor the formation of highly branched, high molecular-weight products and, occasionally, bulky polynuclear aromatics, which lead to a faster catalyst deactivation and lower quality diesel as compared to medium-pore zeolites[31-33].

In a recent paper, the group of Iglesia rationalizes the effects of shape, size and connectivity of channels and cavities of different frameworks in terms of different descriptors, such as the true oligomer selectivity parameter[34]. They conclude that the zeolite structure has not a direct effect on the skeletal structure of the products, but that it does influence the product chain growth and the ability of the primary "true" oligomers to diffuse out of the crystals without being involved in undesired secondary isomerization and β-scission reactions. Thus, sterical limitation towards the formation of chains larger than the dimensions of the pores in 1D zeolites such as TON or MOR is the reason behind their high oligomerization over β-scission selectivity. On the other hand, 3D zeolites such as MFI, BEA or FAU, with cavities and/or channel intersections, will favor the formation of oligomers with sizes too large to diffuse through the channels, which are, therefore, cracked into smaller oligomers. Thus, on large pore, 3D zeolites, undesired secondary reactions such as isomerization, cracking and hetero-oligomerization of these smaller

product alkenes with the reactants, are expected to give a broader product distribution, far from true oligomerization.

Recently, the 1-butene oligomerization rate on H-beta zeolites was shown to be controlled by the diffusion of the oligomers out of the micropores[25] leading to the production of heavier products than with medium pore ZSM-5, as observed also in previous papers by Yoon et al.[35-36] From the study, performed in the liquid phase under industrially relevant conditions, it was concluded that when diffusion is slower than reaction, the longer time spent within the zeolite structure will increase the number of oligomerization steps and, therefore, the molecular weight of the products[25]. This would also increase the probability for isomerization and/or cracking reactions. However, if diffusion path lengths were substantially reduced within 3D large-pore zeolites such as Beta, true oligomers formed would be able to egress the micropore structure before being involved in secondary events. This has already been observed in the case of mesoporous solid acids[34] and hierarchical mordenite[33]. Moreover, it could be expected that, in those cases, the probability to form undesired bulky aromatics would be mostly reduced[25]. The positive effect of shorter diffusion paths would be even more important when converting larger olefins (i.e. $C_5^=$), due to their higher potential for formation of larger products, which could enhance the zeolite pore-blocking [37-38].

Recently, we have described an efficient method to synthesize nanosized large pore Beta zeolites with particle sizes comprised between 10 and 15 nm, using simple alkyl-substituted flexible dicationic organic structure directing agents[39]. Moreover, this method allows controlling the Si/Al ratios in the nanosized Beta zeolites, while maintaining excellent synthesis solid yields (above 90%). Preliminary catalytic results in aromatic alkylation reactions demonstrated that these nanosized high-silica Beta zeolites show high

catalytic activity and high stability towards deactivation, performing significantly better than other commercially available nanocrystalline Beta zeolites[39].

Herein, we present the catalytic behavior of these nanosized Beta zeolites for the liquid phase oligomerization of 1-pentene. The specific combination of high Brønsted acidity (Si/Al ~ 15) and very small crystal sizes (~ 10 nm) allows increasing remarkably the 1-pentene conversion, the catalyst lifetime, and the selectivity to larger oligomers -falling into the diesel fraction- while maintaining high levels of "true-oligomerization".

EXPERIMENTAL SECTION

Materials:

The synthesis of the different nanocrystalline Beta zeolites has been carried out following the procedure described previously[39] and has been attempted with two different Si/Al molar ratios (15 and 30) under alkaline and fluoride media (see Table 1), and using the alkyl-substituted dicationic organic structure directing agents (OSDAs) shown in Figure S1. In a typical synthesis, aluminum hydroxide [$Al(OH)_3$, Sigma-Aldrich] was dissolved in an aqueous solution of the OSDA in its hydroxide form. Colloidal silica (Ludox AS-40, Aldrich) was then added, and the mixture was maintained under stirring for 20 minutes. If required, a 10% wt solution of NH_4F (Sigma-Aldrich) was added, and the resultant mixture gel was allowed to reach the desired silica to water ratio by evaporation under stirring. The final gel compositions were: SiO_2 : 0.0167–0.033Al_2O_3 : 0.2–0.4$OSDA(OH)_2$: 0–0.4NH_4F : 3–30H_2O, where OSDA can be one of the dicationic molecules shown in Figure S1. Finally, the gels were transferred to Teflon lined stainless autoclaves and heated at 150ºC for 10 days. The solids were recovered by filtration, extensively washed with distilled water, and dried at 90ºC overnight. The samples were

calcined in air at 550ºC for 4 hours. The resultant solid yields have been calculated based on silica + alumina conversion.

A commercial nano-beta, CP811 (Zeolyst Int.) was used in its acid form, as supplied, for comparison purposes.

Characterization

Powder X-ray diffraction (PXRD) measurements were performed with a multisample Philips X'Pert diffractometer equipped with a graphite monochromator, operating at 45 kV and 40 mA, and using Cu Kα radiation (λ = 0.1542 nm). The chemical analyses were carried out on a Varian 715-ES ICP-Optical Emission spectrometer, after solid dissolution in HNO_3/HCl/HF aqueous solution. The morphology of the samples was studied with field emission transmission electron microscopy (TEM) using a JEM 2100F microscope. Textural properties were obtained from the N_2 adsorption–desorption isotherms measured at 77 K with Micromeritics ASAP 2020 apparatus. Infrared spectra were measured with a Nicolet 710 FT IR spectrometer. Pyridine adsorption–desorption experiments were made on self-supported wafers (10 mg cm^{-1}) of original samples previously activated at 400ºC and 10^{-2} Pa for 2 hours. After wafer activation, the base spectrum was recorded and pyridine vapor (6.5 x 10^2 Pa) was admitted into the vacuum IR cell and adsorbed onto the zeolite. Desorption of pyridine was performed under vacuum over three consecutive one-hour periods of heating at 150, 250 and 350ºC, each of them followed by an IR measurement at room temperature. The spectra were scaled according to the sample weight.

Characterization of spent catalysts recovered after six hours on stream at W/F=2.8 $g \cdot h \cdot mol^{-1}$, T=200°C, P = 4.0 MPa and 60% mol olefin in the feed, has been performed by means of thermogravimetric and derivative thermogravimetric (TG-DTG) analyses using

a Netzch SAT409 EP coupled to a thermobalance, charging 1–5 mg of the sample and increasing temperature from ambient conditions to 800ºC under air flow (35 ml min^{-1}) with a heating rate of 10ºC min^{-1}, and a EUROEA elemental analyzer (Eurovector) for determination of the carbon content.

Catalytic tests

The catalytic experiments were performed in a 10-mm internal diameter down-flow stainless-steel fixed-bed reactor at 200 ºC, 4.0 MPa, and space times ranging from 2.8 to 9.1 $g \cdot h \cdot mol^{-1}$. Under these conditions of temperature, pressure and feed composition, the reaction occurs in the liquid phase, as determined by means of the process simulation software package Aspen Plus v8.2 (Peng Robinson thermodynamic model). The zeolites were pelletized, crushed and sieved to recover the particles with sizes in the 0.25-0.42 mm fraction. Then the pelletized samples were diluted with SiC (0.64–0.25 mm) to obtain a bed volume of 4.0 cm^3. The temperature in the catalyst bed was controlled by two independent heating zones, with the corresponding thermocouples properly placed inside the catalytic bed. Before reaction, the catalysts were activated in situ by increasing temperature to 520ºC in N_2 flow (200 ml/min) at a rate of 2.0ºC/min and further calcining in air flow (200 ml/min) at 520ºC for 5 h. Then, the reactor was cooled to the reaction temperature in a flow of N_2 (200 ml/min). The olefinic mixture was fed to the reactor as a liquid by means of a Gilson piston pump, and the pressure was controlled during the reaction by means of a back pressure regulator. 1-pentene was co-fed (in the liquid phase) with *n*-heptane in a 60:40 1-pentene/*n*-heptane molar mixture. The full reactor outlet stream was vaporized and analyzed with an online Varian 3400 gas chromatograph. The unconverted reactants and products were separated in a 60 m, 0.25 x 0.25 TRB-5 column and quantified by means of a FID detector. n-Heptane was used as internal standard for mass balance quantification. Finally, the C_{5+} mixture was condensed for further analysis

by simulated distillation, excluding *n*-heptane from the naphtha fraction. For discussion, the selectivity results are referred to by the naphtha, diesel, and heavy product fractions, determined by simulated distillation according to the following cut points:

- Naphtha: C_5–173.9 ºC.
- Diesel: 173.9–391.1 ºC.
- Heavy fraction: 391.1–1000 ºC.

RESULTS AND DISCUSSION

Catalyst characterization

The synthesis of the different nanocrystalline Beta zeolites has been carried out under the conditions summarized in Table 1. As shown there, four nano-Betas have been prepared varying the Si/Al molar ratios (15 and 30) and the synthesis media (alkaline and fluoride), and using the organic molecules shown in Figure S1 as OSDAs. The PXRD patterns of the solids obtained after the hydrothermal crystallization reveal the formation of Beta zeolite in all cases (see Figure 1). Moreover, the very broad diffraction peaks observed there for Beta-15-OH, Beta-15-F and Beta-30-OH samples, suggest that these materials may present smaller crystallites than Beta-30-F sample. This fact is confirmed by TEM microscopy, and the images enclosed in Figure 2 show that the crystal sizes of Beta-15-OH, Beta-15-F and Beta-30-OH samples are ~10-15 nm, whereas the crystal size of Beta-30-F is ~30-40 nm. In good agreement with their reduced crystal sizes, and as determined from the corresponding N_2 isotherms (see Figure S2) Beta-15-OH, Beta-15-F and Beta-30-OH show larger BET and external surface areas (~720-750 and 400-490 m^2/g, respectively, see Table 2) than Beta-30-F (~570 and 240 m^2/g, see Table 2). Still, the samples synthesized in alkaline media present larger BET and external surface areas

suggesting smaller crystal sizes than those of the zeolites prepared in the presence of fluoride with comparable Al content.

Regarding the chemical composition of these different nanosized Beta zeolites, their ICP analyses indicate that the theoretical Si/Al molar ratios introduced in the initial synthesis gels (15 or 30, see Table 1) remain almost intact in the final solids (~15-16 or 29-30, see Table 2).

Zeolites synthesized in fluoride media, as compared to zeolites prepared in alkaline media, are known to be more hydrophobic, mainly due to their larger crystal size and reduced number of defects, and especially in the case of high silica zeolites [REF???]. Regarding the different hydrophilic/hydrophobic nature of the Beta-F and Beta-OH zeolites presented in this work, we believe the differences between the two nanobetas of Si/Al=15 should not be very large, due to their small crystal size. In fact, they both present an intense peak at 3750 cm^{-1} in the FT-IR spectra (presented now as Figure S3 in the Supplementary Information) assigned to external silanols, in good agreement with their high external surface areas. A similar spectrum was obtained for Beta-30-OH, despite its lower Al content. Thus, these three samples should present comparable hydrophilicity. On the other hand, sample Beta-30-F, with a larger crystal size, presents a reduced size of the external Si-OH peak. The reduced external surface area and the smaller amount of external Si-OH will confer this sample a more hydrophobic nature.

The Brønsted acidity of these materials has been measured by FTIR spectroscopy combined with adsorption of pyridine and desorption of the probe at increasing temperatures (150, 250 and 350ºC). The FT-IR spectra of the adsorbed pyridine obtained for the nanosized Betas and the commercial reference CP811 are shown in Figure S4 and the corresponding Brønsted and Lewis acidity are enclosed in Table 3. As expected, the

nanosized Beta zeolites with Si/Al ratios of ~15, Beta-15-OH and Beta-15-F, present higher Brønsted acid site density than the nanosized Beta zeolites with Si/Al molar ratios of ~30, Beta-30-OH and Beta-30-F, for the three desorption temperatures studied (see T=150, 250 and 350ºC in Table 3), as could be expected from the higher Al content of the two former.

Besides the nanocrystalline Beta zeolites described so far, a commercially available nanosized Beta zeolite (CP811, Zeolyst) has also been considered for comparison purposes. This material has a Si/Al molar ratio of ~12 and an average particle size of ~30 nm (see TEM image in Figure 2). The measured BET and external surface areas are 580 and 203 m^2/g, respectively, as shown in Table 2, values that are comparable to those obtained for the Beta-30-F sample, with a similar crystal size (~30-40 nm, see Figure 2). Finally, the commercially available nanosized Beta zeolite shows a higher total Brønsted acidity than Beta-15-OH and Beta-15-F at low pyridine desorption temperatures (see T=150ºC in Table 3), in good agreement with its lower Si/Al ratio, but similar amount of retained pyridine molecules when desorbing at higher temperatures (see T=350ºC in Table 3), indicating a different acid strength distribution.

Catalytic oligomerization of 1-pentene.

As shown in the previous section, samples Beta-15-OH and Beta-15-F present comparable crystal size, textural and acidic properties despite being prepared by means of different procedures (alkaline and fluoride media), and Beta-15-OH and Beta-30-OH present comparable crystal size and textural properties but different amount of Brønsted acid sites. Beta-15-F and Beta-30-F differ in both, crystal size and acidity, but the crystallites of the latter are comparable in size to those of the commercial reference CP811, which has a significantly larger Brønsted acid site density. Thus, comparison of

the catalytic behavior of this set of nano-betas will allow the determination of the influence of number of active sites on initial activity, deactivation rate and product selectivity for zeolites with crystal sizes in two different ranges, below 15 nm for Beta-15-OH, Beta-15-F and Beta-30-OH, and in the 30-40 nm range for Beta-30-F and CP811.

The oligomerization of 1-pentene to liquid fuels has been evaluated under industrially relevant liquid phase conditions, at 200°C and 4.0 MPa, and at three different space times, W/F = 9.1, 4.9 and 2.8 $g \cdot h \cdot mol^{-1}$, referred to the olefin. 1-Pentene conversion at W/F=9.1 $g \cdot h \cdot mol^{-1}$ is shown in Figure 3A. The first thing to be noted is the significantly higher activity and stability towards deactivation of the three nanosized Beta zeolites with smaller crystal sizes (10-15 nm) and larger external surface areas, Beta-15-OH, Beta-30-OH and Beta-15-F, as compared to the commercial beta, CP811 and Beta-30-F, both with crystal sizes in the range of 30-40 nm. The two latter catalysts present high initial activity but they differ in their deactivation rate at increasing time on stream (TOS). Thus, the commercial reference CP811, with a larger amount of Brønsted acid sites, presents a higher stability towards deactivation as compared to Beta-30-F, with a considerably lower Brønsted acid site density (see Table 3), in good agreement with previous results obtained with ZSM-5 zeolites[18].

In order to see differences among the three most active nanobetas, space time is decreased from 9.1 to 4.9 and 2.8 $g \cdot h \cdot mol^{-1}$ (Figures 3B and 3C, respectively). Under these more severe conditions, the two nanosized betas with Si/Al ratios of 15 are the most active, with the sample synthesized in OH media being slightly more active than the zeolite obtained in F media. These differences in activity can be due to small differences in the crystal size. Although the TEM images (see Figure 2) do not show clear differences in the crystallite size of these two nanobetas, the larger BET and external surface area of Beta-15-OH as compared to Beta-15-F (757.4 and 489.9 m^2/g vs 719.8 and 323.6 m^2/g,

see Table 2) points out to a smaller crystal size of the former. Beta-30-OH, with comparable nanosized crystallites and external surface area, but with lower amount of total and strong acid sites, presents a faster deactivation when compared at the lowest space time of 2.8 $g \cdot h \cdot mol^{-1}$, due to the reduced number of active sites. This is in good agreement with previous results[18] that showed that when crystalline diffusion path lengths were reduced below a certain critical level, the higher the amount of Brønsted acid sites, the higher the olefin conversion. It is important to remark the much higher activity presented by the three nanosized Beta zeolites as compared to the other two catalysts, Beta-30-F and CP811. The conversion values obtained with the former exceeds the conversion level obtained with the zeolites with larger crystal size at a threefold space time.

As shown in Figure 4, the initial product selectivity greatly depends on the physico-chemical properties of the nanosized Beta zeolites tested. However, different selectivity trends are also observed when the catalysts are compared at the different space times. Thus, when compared at the highest space time of 9.1 $g \cdot h \cdot mol^{-1}$ (Figure 4A), the three most active nano-crystalline beta zeolites, Beta-15-OH, 30-OH and 15-F, with similar crystal sizes of 10-15 nm, present increased selectivity to naphtha and lower selectivity to diesel when increasing the Brønsted acid site density, at comparable olefin conversions around 90%. However, considering all the samples studied, the highest selectivity to naphtha is obtained for the commercial beta, CP811, which has the largest amount of Brønsted acid sites and a larger crystal size, in the range of 30-40 nm. Under these conditions of higher space time, secondary conversion of the primary oligomers (isomerization and cracking) could be expected to contribute to the final product distribution obtained with beta catalysts[34], especially during the initial stage of the reaction, when the catalysts are less deactivated. However, when looking at the product

distribution within the liquids collected during the first three hours on stream, it does not deviate much from what could be considered as true oligomerization[19] (see the typical shape for dimers and trimers in Figure S5). Moreover, the on-line analysis do not evidence a significant formation of lighter products, which could come from β-scission events, for any of the catalysts, and selectivity to gases is kept below 5 wt% in all cases, including the commercial beta, CP811. Thus, the lower selectivity to diesel range molecules of this catalyst, under our conditions, is not due to cracking of the bulkier oligomers, but can only be explained by the non-diffusion of these bulkier molecules out of the zeolite structure. The larger number of active sites and the longer diffusional path lengths in CP811, as compared to Beta-15-OH, 30-OH and 15-F, will favor consecutive oligomerization reactions to products that will not be able to egress the crystals.

Although the same can be applied to the smaller nanosized betas, their reduced number of active sites will limit the number of oligomerization steps, and therefore the growing of the products, and their diffusion out of the zeolite structures will be facilitated by the shorter diffusion paths. Thus, the different selectivity to naphtha in the liquid products observed for the five beta zeolites can be ascribed to the non-egression of the larger oligomers at these high space times, and can be correlated with the amount of acid sites and crystal sizes of the nano-zeolites. In fact, at higher times on stream (TOS) where the catalysts are, at least, partially deactivated, and the number of active sites participating in the reaction will be lower, the selectivity to diesel increases (see results for TOS=3-6 h in Figure 5A). The low extension of cracking of the large, bulky oligomers formed within the zeolite micropores can be explained by the reaction temperature used here, of 200ºC, which is considered the upper limit for performing selective oligomerization with low cracking contribution[19].

The selectivity differences change, however, when reducing the space time to 4.9 and 2.8 $g \cdot h \cdot mol^{-1}$ (see Figures 4B, 4C, 5B and 5C). Under these conditions of higher throughput, the contribution of secondary –undesired- reactions is expected to be significantly lower, and we observe a higher selectivity to diesel, especially at the intermediate space time, for zeolites Beta-15-OH and Beta-15-F, with the smallest crystal size and the highest Brønsted acid site density. The reduced crystal size leads to improved mass transport and a more efficient use of the zeolite crystals, shifting the oligomer distribution towards heavier products. The same was observed when comparing the product distribution obtained with a purely microporous mordenite and with a micro-mesoporous mordenite obtained by post-synthesis desilication, where the latter was more selective to heavier oligomers, which could desorb and diffuse easier due to the reduced diffusion path lengths[33]. Lowering the number of active sites (Beta-30-OH) while keeping the crystals in the 10-20 nm range results in a lower selectivity to diesel range molecules (trimers or tetramers), which need at least two consecutive oligomerization steps to be formed. On the other hand, increasing crystal size has a different effect depending on the amount of active sites. So, the selectivity to diesel obtained with the less acidic Beta-F-30 decreases with space time, confirming that the low selectivity to naphtha in this case is due to the lower Brønsted acid site density and the limited number of successive oligomerization steps. However, the selectivity to diesel increases for the commercial Beta when decreasing the space time, indicating that the higher throughput limits the number of oligomerization steps and favors the formation and egression of diesel range compounds. The experiments performed at the different space times allow us to compare selectivity within the liquid products obtained with the nanosized Beta-15-OH and Beta-15-F and the commercial CP811 beta at comparable initial conversion and deactivation rates (W/F of 2.8 and 9.1 $g \cdot h \cdot mol^{-1}$, respectively). When compared under those conditions

of similar activity, the two nanosized zeolites Beta-15-OH and Beta-15-F are more selective to diesel than the reference beta CP811, despite the higher space time used in the case of the latter, which is expected to favor the formation of larger oligomers. Thus, the reduced crystal size of the nanosized beta zeolites synthesized as described here, is determinant for the larger selectivity to oligomers in the diesel range.

Characterization of spent catalysts.

In order to study more thoroughly the possible deactivation causes of the different nano-betas and the type of carbonaceous species formed in each case, the spent catalysts have been recovered after six hours on stream at W/F=2.8 $g \cdot h \cdot mol^{-1}$, T=200°C, P = 4.0 MPa and 60% mol olefin in the feed, and characterized by means of Elemental Analysis and TG-DGT measurements. According to the results enclosed in Tables 4 and 5, the three most active nanosized betas, Beta-15-OH, 30-OH and 15-F, present comparable amounts of carbonaceous residues on the catalysts (around 12-13 wt%) and comparable distribution of the type of these residues. Indeed, three weight losses can be observed in Figure 6A, and two peaks can be differentiated associated to carbon species on the catalysts (Figure 6B). The one at lower temperature (around 280°C) has been assigned to adsorbed oligomers, and the second peak, at higher temperature, corresponds to heavier coke species, burning off at temperatures above 400°C[18]. However, the H/C molar ratio of these carbon species is higher (around 2, typical of a mono-olefin) for zeolite Beta-30-OH, with the lowest Brønsted acid site density (see Table 4). The total amount of coke on Beta-30-F, with larger crystal and lower amount of active sites, is slightly lower than for the rest of the synthesized nanobetas. It has an H/C ratio close to 2, and the proportion of carbon due to adsorbed hydrocarbons is higher (close to 60%), in good agreement with a lower number of oligomerization steps taking place, and with higher diffusional

problems. However, a larger amount of carbonaceous species was found on the commercial CP811, with bigger crystals and the highest amount of acid sites, species with a lower H/C molar ratio (1.6) and a larger proportion of the true coke (66 wt% vs. 50-58 for the other zeolites). The color of the spent samples is also in good correlation with the type and nature of the carbonaceous species described (see Figure S6). Thus, the results obtained are in line with the catalytic results discussed so far. For the beta zeolites with high acidity (Si/Al=12-15), the reduced crystal size of Beta-15-OH and Beta-15-F (10-15 nm) limits the number of oligomerization steps and the formation of heavier coke species as compared to the commercial CP811, as a consequence of a faster egression of the dimers and/or trimers formed. On the other hand, for comparable crystal sizes, the higher the number of Brønsted acid sites, the higher the proportion of hard coke and the lower the H/C molar ratio of the coke, due to a larger extension of consecutive oligomerization reactions leading to bulkier coke precursors.

If the carbon residues formed on the nanosized beta zeolites is the only responsible for the progressive activity loss, their catalytic activity could be restored by combustion of these carbon species. The possible regeneration by *in-situ* calcination at 540ºC for 5 hours has been studied for the nanosized Beta-15-OH and Beta-15-F zeolites tested at W/F=2.8 and 9.1 $g \cdot h \cdot mol^{-1}$, respectively. The catalytic behavior of these two samples regenerated after three consecutive oligomerization-regeneration experiments was evaluated at the same space times, and compared with that of the fresh nano-betas in Figure S7. The results presented show that the regenerated nano-betas not only maintain similar catalytic activities than fresh catalysts (see Figure S6A), but also comparable product selectivities (see Figure S6B), indicating their high hydrothermal stability.

Conclusions

Nanocrystalline Beta zeolites with very low crystal sizes (~ 10-15 nm) and controlled Brønsted acidity, synthesized in the presence of simple alkyl-substituted flexible dicationic OSDAs, perform as efficient heterogeneous acid catalysts for the selective oligomerization of pentene into liquid fuels. The combination of an optimum Brønsted acid site density and very short diffusional path lengths confers these nanosized Betas high initial activity and significantly improved stability towards deactivation with TOS as compared to a commercial nanobeta with a larger crystal size (~ 30 nm) at high space times (W/F=9.1 $g \cdot h \cdot mol^{-1}$). The differences are even more noticeably when the catalysts are tested under more severe conditions (W/F=2.8 $g \cdot h \cdot mol^{-1}$). In fact, at these higher throughputs, the commercial beta presents olefin conversion below 30% after 3 hours TOS, whereas the synthesized nanobetas maintain 1-pentene conversions around 80% after 6 hours on stream. The nanobetas synthesized with reduced crystal size present also higher selectivity to diesel as compared to commercially available nanosized Beta catalysts, not only at the highest space times, but also when compared at similar conversion levels. Finally, the synthesized nanocrystalline Beta zeolites present high resistance against catalyst deactivation with TOS, with excellent regenerability and reusability.

ASSOCIATED CONTENT: SUPPORTING INFORMATION

Supporting Information Available: OSDAs used for the synthesis of the nanobetas, additional characterization of fresh and spent catalysts, product distribution within the liquid products as determined by simulated distillatio and results on regenerability tests. This material is available free of charge via the Internet at http://pubs.acs.org

ACKNOWLEDGMENTS

Financial support by the Spanish Government-MINECO through ‘‘Severo Ochoa” (SEV-2016-0683), MAT2015-71261-R and CTQ2015-70126-R, by the Fundación Ramón Areces through a research project within the “Life and Materials Sciences” program, and by the European Union through ERC-AdG-2014-671093 – Syn-CatMatch is acknowledged. M.R.D-R. acknowledges “La Caixa - Severo Ochoa” International PhD Fellowships (call 2015). The Electron Microscopy Service of the Universitat Politècnica de València is acknowledged for their help in sample characterization.

.

REFERENCES

1. Peratello, S.; Molinari, M.; Bellussi, G.; Perego, C., *Catal. Today* **1999**, *52*, 271-277.
2. Martinez, C.; Corma, A., *Coord. Chem. Rev*. **2011**, *255*, 1558-1580.
3. Muraza, O., *Ind. Eng. Chem. Res*. **2015**, *54*, 781-789.
4. Corma, A.; Corresa, E.; Mathieu, Y.; Sauvanaud, L.; Al-Bogami, S.; Al-Ghrami, M. S.; Bourane, A., *Catal. Sci. Technol*. **2017**, *7*, 12-46.
5. de Klerk, A.; Maitlis, P. M., What Can We Do with Fischer-Tropsch Products? In Greener Fischer-Tropsch Processes for Fuels and Feedstocks, Wiley-VCH: **2013**; pp 81-105.
6. Zakaria, Z. Y.; Linnekoski, J.; Amin, N. A. S., *Chem. Eng. J.* **2012**, *207–208*, 803-813.
7. Wang, Q.; Chen, X.; Jha, A. N.; Rogers, H., *Renew. Sust. Energy Rev*. **2014**, *30*, 1-28.
8. Schmidt, R.; Welch, M. B.; Randolph, B. B., *Energy Fuels* **2008**, *22*, 1148-1155.
9. Ipatieff, V. N.; Corson, B. B.; Egloff, G., *Ind. Eng. Chem*. **1935**, *27*, 1077-1081.
10. O'Connor, C. T., Energy-Related Catalysis: Aromatization of Light Alkanes. In Handbook of Heterogeneous Catalysis, Wiley-VCH Verlag GmbH: **2008**; Vol. 4-5, pp 2069-2074.
11. Occelli, M. L.; Hsu, J. T.; Galya, L. G., *J. Molec. Catal*. **1985**, *32*, 377-390.
12. Degnan Jr, T. F.; Smith, C. M.; Venkat, C. R., *Appl. Catal. A Gen.* **2001**, *221*, 283-294.
13. Martens, L. R.; Verduijn, J. P.; Mathys, G. M., *Catal. Today* **1997**, *36*, 451-460.
14. Quann, R. J.; Green, L. A.; Tabak, S. A.; Krambeck, F. J., *Ind. Eng. Chem. Res.* **1988**, *27,* 565-570.
15. Catani, R.; Mandreoli, M.; Rossini, S.; Vaccari, A., *Catal. Today* **2002**, *75*, 125-131.
16. Martens, J. A.; Ravishankar, R.; Mishin, I. E.; Jacobs, P. A., *Angew. Chem. Int. Ed.* **2000**, *39*, 4376-4379.

17. Mlinar, A. N.; Zimmerman, P. M.; Celik, F. E.; Head-Gordon, M.; Bell, A. T., *J. Catal*. **2012**, *288*, 65-73.

18. Corma, A.; Martinez, C.; Doskocil, E., *J. Catal*. **2013**, *300*, 183-196.

19. Tabak, S. A.; Krambeck, F. J.; Garwood, W. E., *AIChE Journal* **1986**, *32*, 1526-1531.

20. Csicsery, S. M., Catalysis by shape selective zeolites-science and technology. In *Pure Appl. Chem*., **1986**; Vol. *58*, p 841.

21. Vermeiren, W.; Gilson, J.-P., *Top. Catal*. **2009**, *52*, 31.

22. Coelho, A.; Caeiro, G.; Lemos, M. A. N. D. A.; Lemos, F.; Ribeiro, F. R., *Fuel* **2013**, *111*, 449-460.

23. Popov, A. G.; Fedosov, D. A.; Ivanova, I. I.; Vedernikov, O. S.; Kleimenov, A. V.; Kondrashev, D. O.; Miroshkina, V. D.; Abrashenkov, P. A.; Kuznetsov, S. E., *Petrol. Chem*. **2016**, *56*, 237-243.

24. Moliner, M.; Martínez, C.; Corma , A., *Angew. Chem. Int. Ed.* **2015**, *54*, 3560-3579.

25. Wulfers, M. J.; Lobo, R. F., *Appl. Catal. A Gen*. **2015**, *505*, 394-401.

26. Bellussi, G.; Mizia, F.; Calemma, V.; Pollesel, P.; Millini, R., *Microporous Mesoporous Mater*. **2012**, *164*, 127-134.

27. Martinez, C.; Doskocil, E. J.; Corma, A., *Top. Catal*. **2014**, *57*, 668-682.

28. Popov, A. G.; Pavlov, V. S.; Ivanova, I. I., *J. Catal*. **2016**, *335*, 155-164.

29. Kulkarni, A.; Kumar, A.; Goldman, A. S.; Celik, F. E., *Catal. Commun*. **2016**, *75*, 98-102.

30. Flego, C.; Marchionna, M.; Perego, C., High quality diesel by olefin oligomerisation: new tailored catalysts. In Stud. Surf. Sci. Catal., J. Čejka, N. Ž.; Nachtigall, P., Eds. Elsevier: **2005**; Vol. Volume 158, Part B, pp 1271-1278.

31. Miller, S. J., Olefin Oligomerization Over High Silica Zeolites. In Stud. Surf. Sci. Catal., Ward, J. W., Ed. Elsevier: **1988**; Vol. Volume 38, pp 187-197.

32. Pater, J. P. G.; Jacobs, P. A.; Martens, J. A., *J. Catal*. **1998**, *179*, 477-482.

33. Bertrand-Drira, C.; Cheng, X.-w.; Cacciaguerra, T.; Trens, P.; Melinte, G.; Ersen, O.; Minoux, D.; Finiels, A.; Fajula, F.; Gerardin, C., *Microporous Mesoporous Mater*. **2015**, *213*, 142-149.

34. Sarazen, M. L.; Doskocil, E.; Iglesia, E., *ACS Catal*. **2016**, *6*, 7059-7070.

35. Yoon, J. W.; Chang, J.-S.; Lee, H.-D.; Kim, T.-J.; Jhung, S. H., *J. Catal*. **2007**, *245*, 253-256.

36. Yoon, J. W.; Jhung, S. H.; Choo, D. H.; Lee, S. J.; Lee, K.-Y.; Chang, J.-S., *Appl. Catal. A Gen.* **2008**, *337*, 73-77.

37. Van Grieken, R.; Escola, J. M.; Moreno, J.; Rodriguez, R., *Appl. Catal. A Gen*. **2006**, *305*, 176-188.

38. de Klerk, A., *Ind. Eng. Chem. Res.* **2005**, *44*, 3887-3893.

39. Martinez-Franco, R.; Paris, C.; Martinez-Armero, M. E.; Martinez, C.; Moliner, M.; Corma, A., *Chem. Sci.* **2016**, *7*, 102-108.

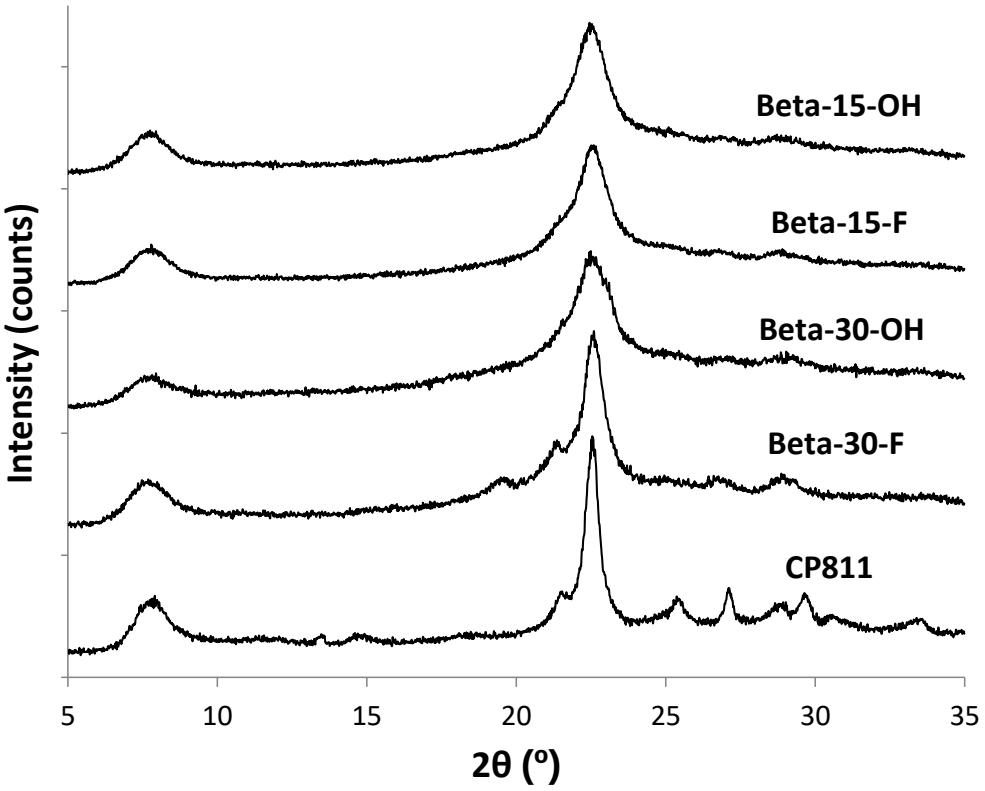

Figure 1: PXRD patterns of the as-prepared nanosized Beta zeolites

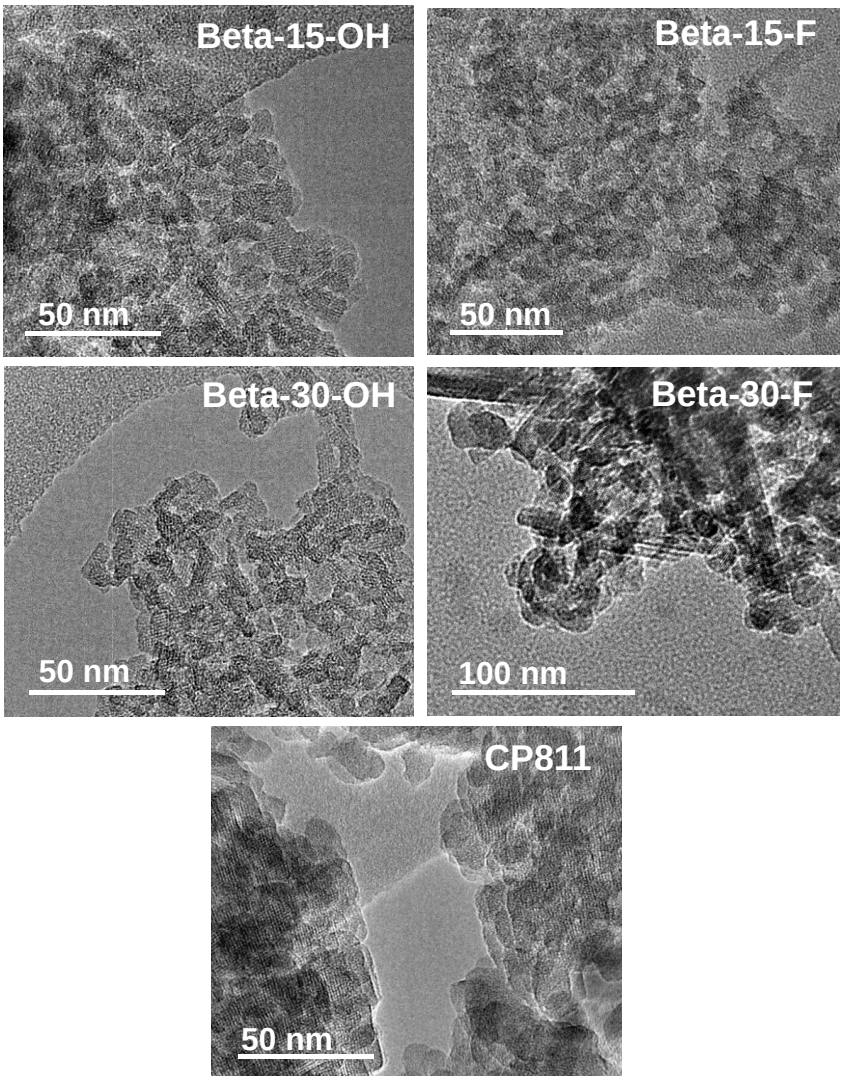

Figure 2: TEM images of the nanosized Beta zeolites

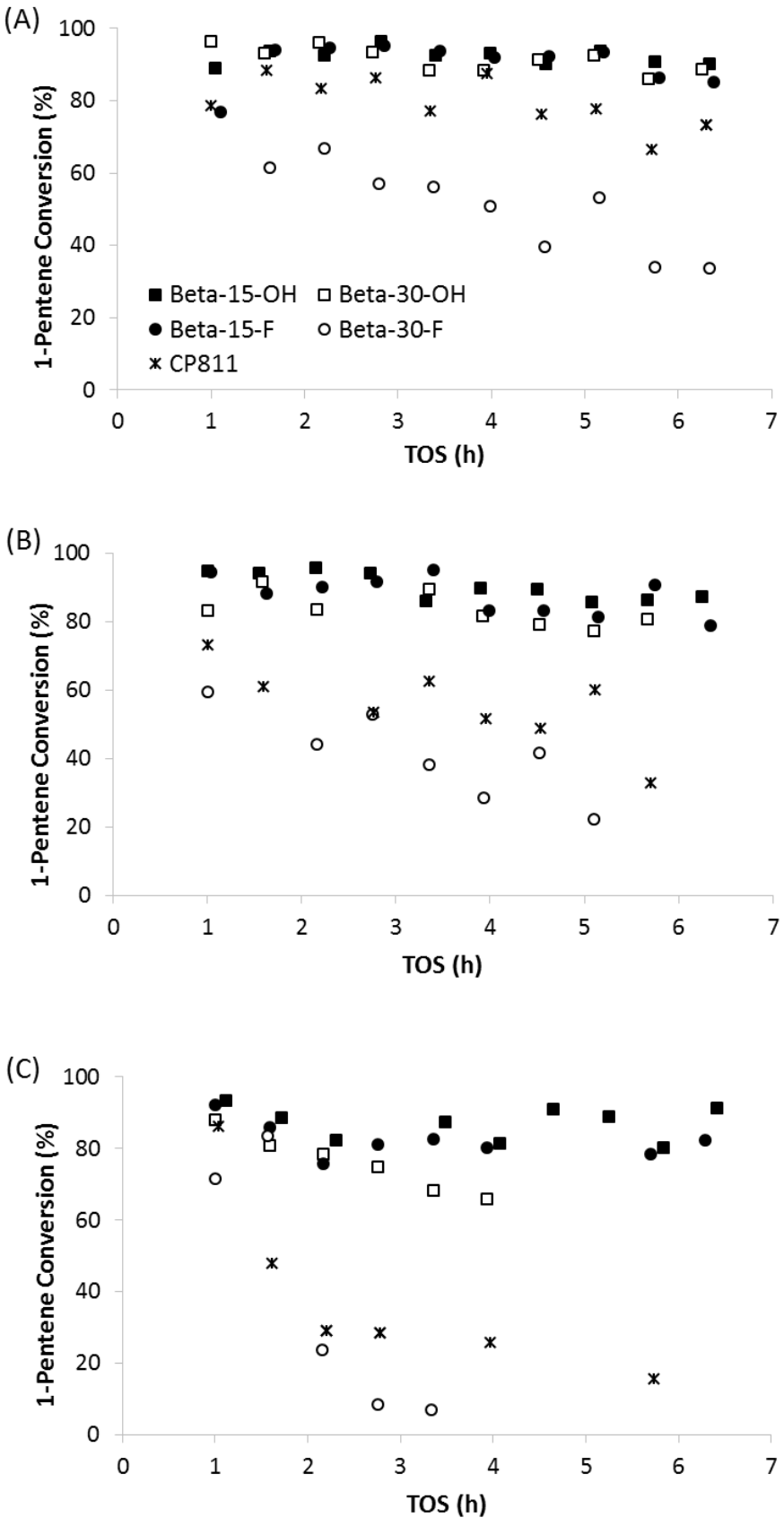

Figure 3: 1-Pentene conversion vs. TOS for nanosized Beta catalysts at W/F = 9.1 (A), 4.9 (B) and 2.8 (C) $g \cdot h \cdot mol^{-1}$. T=200°C, P = 4.0 MPa, 60% mol olefin in the feed.

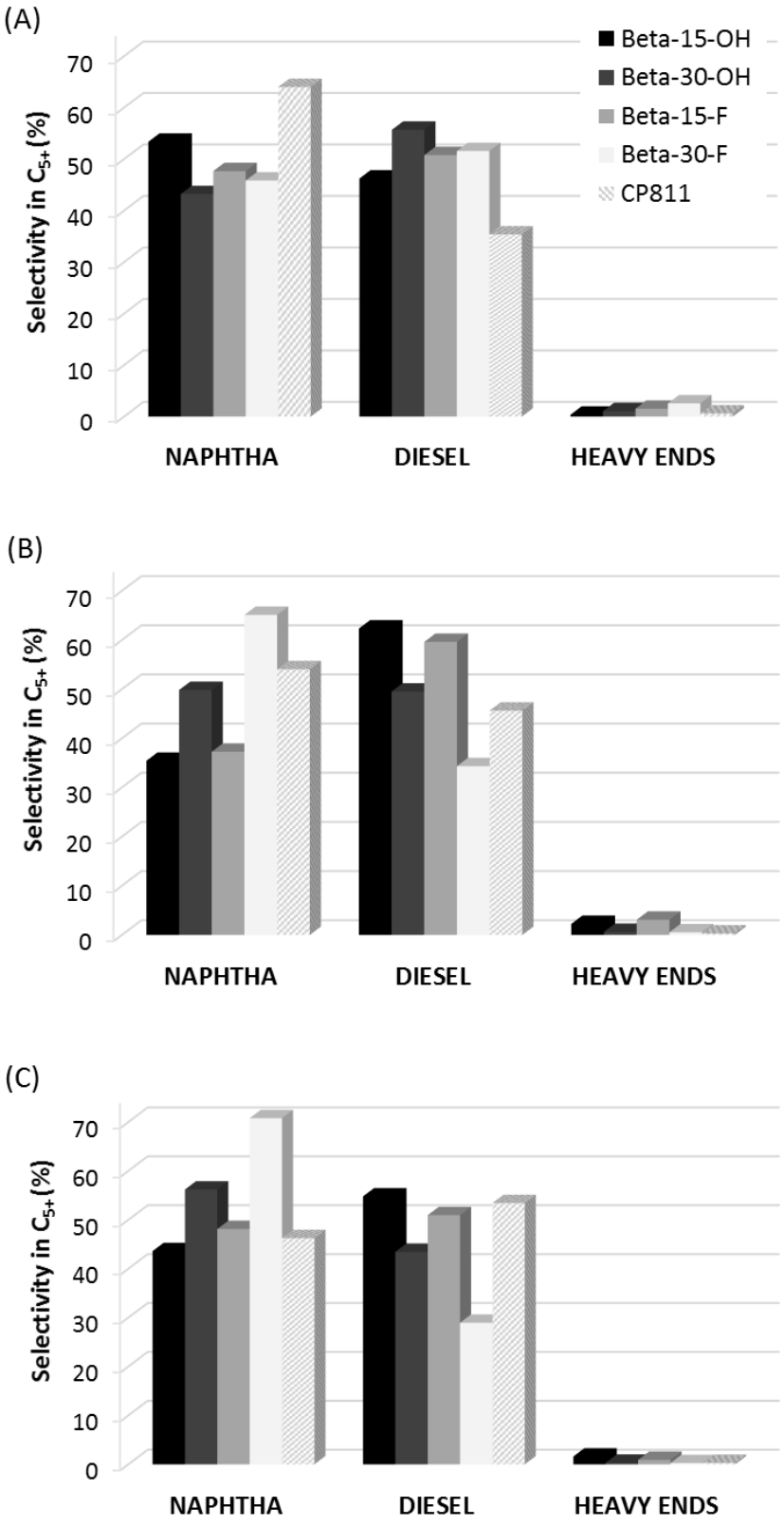

Figure 4: Selectivity within the C_{5+} liquid fractions accumulated during the first three hours TOS (0-3 h) for the nano-sized Beta catalysts at W/F = 9.1 (A), 4.9 (B) and 2.8 (C) $g \cdot h \cdot mol^{-1}$. T=200°C, P = 4.0 MPa, 60% mol olefin in the feed.

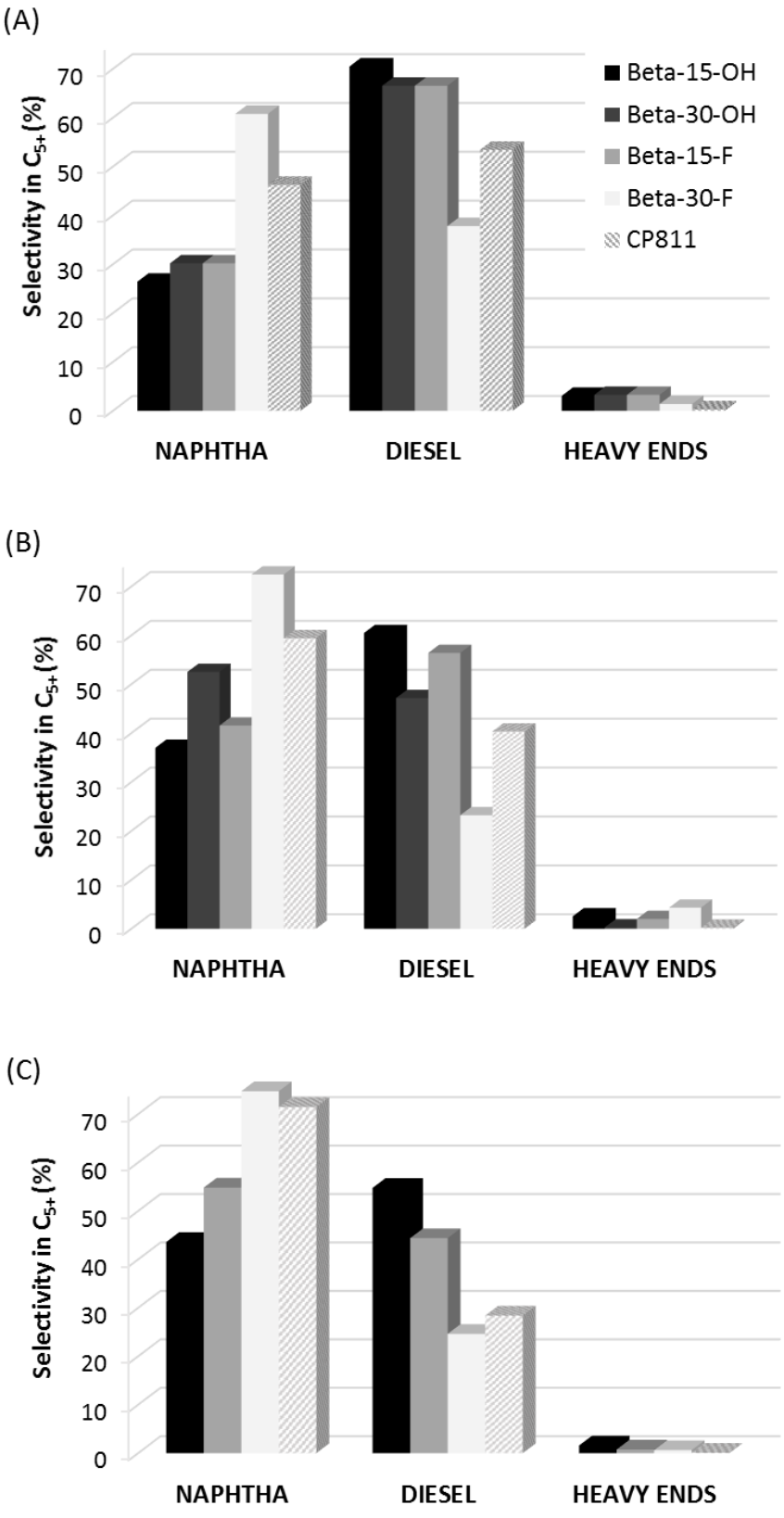

Figure 5: Selectivity within the C_{5+} liquid fractions accumulated during the last three hours TOS (3-6 h) for the nano-sized Beta catalysts at W/F = 9.1 (A), 4.9 (B) and 2.8 (C) $g \cdot h \cdot mol^{-1}$. T=200°C, P = 4.0 MPa, 60% mol olefin in the feed.

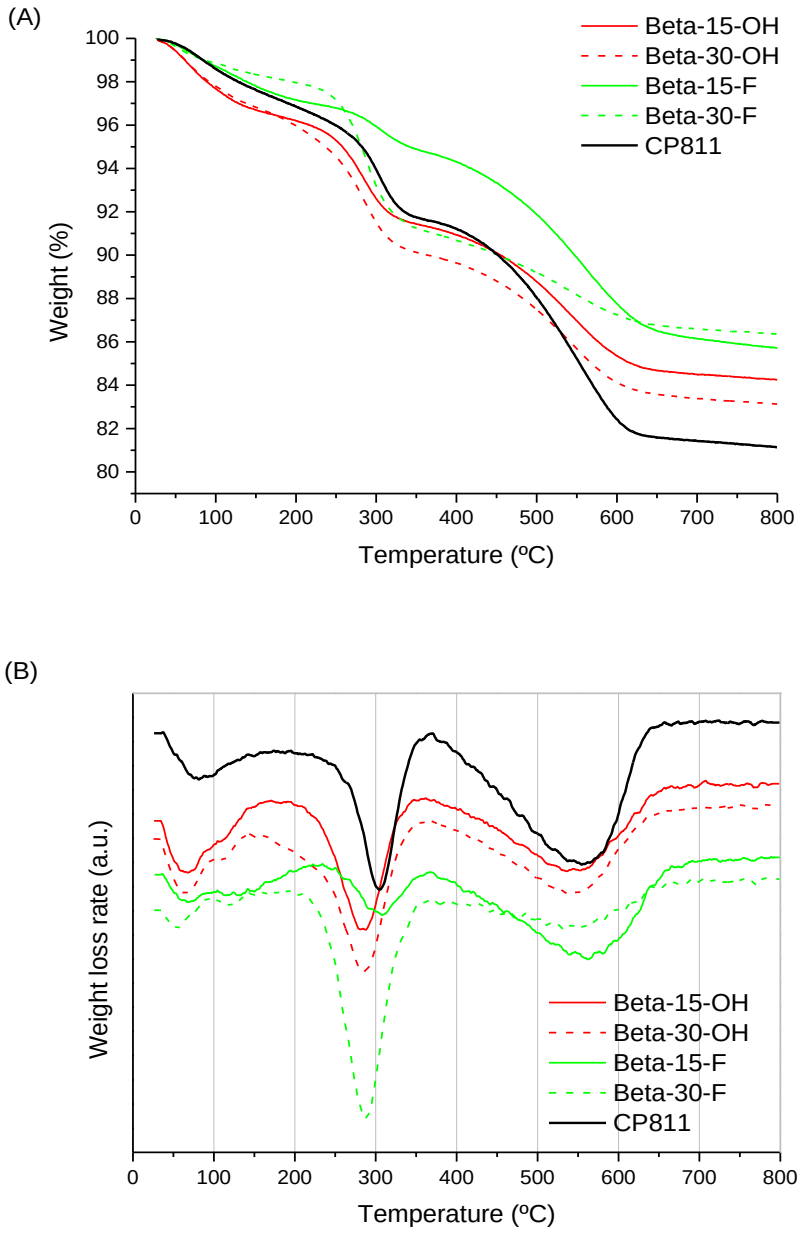

Figure 6: TG (a) and DTG (b) profiles of spent beta catalysts, obtained after 1-pentene oligomerization at W/F=2.8 g·h·mol^{-1}, T=200°C, P = 4.0 MPa and 60% mol olefin in the feed.

Table 1: Synthesis conditions for the different nanocrystalline Beta zeolites. Their crystallization has been carried out at 150ºC for 10 days.

Sample	**OSDA**	**Si/Al[a]**	**OSDA/Si[a]**	**H_2O/Si[a]**	**F/Si[a]**
Beta-15-OH	OSDA-C4	15	0.4	10	-
Beta-30-OH	OSDA-C6	30	0.4	10	-
Beta-15-F	OSDA-C4	15	0.25	15	0.25
Beta-30-F	OSDA-C4	30	0.4	3	0.4

[a] Molar ratios

Table 2: Chemical analysis and textural properties of the nanosized Beta zeolites in their calcined form measured by N_2 adsorption/desorption

Sample	Si/Al)$_{ICP}$	Area BET (m^2/g)	External surface area (m^2/g)[a]	Micropore area (m^2/g) [a]	Micropore volume (cm^3/g) [a]
Beta-15-OH	15.3	757.4	489.9	317.5	0.15
Beta-30-OH	30.6	738.2	428.7	309.5	0.14
Beta-15-F	16.0	719.8	396.2	323.6	0.15
Beta-30-F	29.8	568.5	241.1	327.4	0.16
CP811	11.0	580.0	203.1	378.4	0.18

[a] External surface area, micropore area and micropore volume determined from t-plot.

Table 3: Acidity of nanosized Beta zeolites as determined by FT-IR combined with pyridine adsorption-desorption

Sample	Acidity (µmol pyridine/g)					
	Brønsted			Lewis		
	T=150ºC	T=250ºC	T=350ºC	T=150ºC	T=250ºC	T=350ºC
Beta-15-OH	146	130	94	68	64	52
Beta-30-OH	110	98	47	84	82	71
Beta-15-F	163	144	88	87	75	71
Beta-30-F	71	53	23	24	21	19
CP811	220	165	85	211	205	193

Table 4: Coke amount (wt%) and H/C molar ratio determined by Elemental Analysis for the spent beta catalysts obtained after 1-pentene oligomerization at W/F=2.8 $g \cdot h \cdot mol^{-1}$, T=200°C, P = 4.0 MPa and 60% mol olefin in the feed.

Sample	Coke (wt%)	H/C molar ratio
Beta-15-OH	13.4	1.8
Beta-30-OH	12.7	2.1
Beta-15-F	12.8	1.6
Beta-30-F	11.3	2.0
CP811	15.6	1.6

Table 5: Coke amount (wt%) and coke distribution into soft coke (adsorbed oligomers, burning off at a temperature around 280°C) and hard coke (burning off at temperatures above 400°C) determined by TG-DTG for the spent beta catalysts obtained after 1-pentene oligomerization at W/F=2.8 $g \cdot h \cdot mol^{-1}$, T=200°C, P = 4.0 MPa and 60% mol olefin in the feed.

Sample	Coke (wt%)	Soft coke (wt%)	Hard coke (wt%)	Soft coke (%)	Hard coke (%)
Beta-15-OH	12.2	5.1	7.1	41.8	58.2
Beta-30-OH	13.7	6.8	6.9	49.6	50.4
Beta-15-F	12.8	5.4	7.4	41.8	58.2
Beta-30-F	11.7	6.7	4.9	57.7	42.3
CP811	15.8	5.3	10.4	33.8	66.2

TOC